The Excited State Equilibrium between Two Rotational Conformers of a Sterically Restricted Donor−Acceptor Biphenyl As Characterized by Global Fluorescence Decay Analysis†

Michael Maus and Wolfgang Rettig*

W. Nernst-Institut für Physikalische und Theoretische Chemie, Humboldt-Universität zu Berlin, Bunsenstrasse 1, D-10117 Berlin, Germany

Received: June 26, 2001; In Final Form: September 12, 2001

A global fluorescence decay analysis approach has been employed to characterize the conformational relaxation in the excited state of a sterically hindered twisted donor−acceptor biphenyl (**III**) dissolved in diethyl ether (EOE). A temperature dependent population ratio of two conformationally different charge-transfer species CT and CTR is found for which the thermodynamic equilibration (reversible photoreaction) is reached above 265 K. The separated fluorescence bands of CT and CTR as well as kinetic and thermodynamic parameters associated with the adiabatic (forward and backward) photoreaction could be determined ($\Delta H = -2.5$ kJ/mol, $\Delta S = -0.7$ J/(mol K) with activation barriers $E_a(\mathrm{CT} \rightarrow \mathrm{CTR}) = 14.3$ kJ/mol and $E_a(\mathrm{CT} \leftarrow \mathrm{CTR}) = 16.8$ kJ/mol). The derived excited state dipole moments ($\mu_{CT} = 26$D; $\mu_{CTR} = 30$D) and their k_f ratio ($k_f^{CTR}/k_f^{CT} \approx 0.7$) are consistent with a photoreaction from a more planar (CT) to a more twisted (CTR) conformer.

1. Introduction

The phenomenon of dual fluorescence has attracted great attention in the past three decades.[1−17] From time to time, new molecules are presented that do not obey Kasha's rule[18] that "*emission always occurs from the lowest electronically excited state of a given multiplicity*". Small Franck−Condon factors and small electronic coupling matrix elements between the relevant higher (S_x) and lowest (S_1) excited diabatic states are frequently discussed as a possible source of dual emission from S_x and S_1.[1−5] Alternative possibilities in accord with Kasha's rule to observe dual fluorescence are adiabatic photoreactions.[6−17] In these cases, a nuclear rearrangement takes place on the adiabatic S_1 hypersurface, which can be slowed by appropriate conditions of the environment to the nanosecond time scale of fluorescence. A well-studied example is 4-(dimethylamino)-benzonitrile (DMABN), which is thought to exist in two stable molecular structures in the excited state.[6−9,11,13−15] The occurrence of well separated dual fluorescence bands in DMABN and derivatives allowed a detailed characterization of the excited state equilibrium parameters by a conventional analysis of single-photon counting and steady state experiments.[10,11,13−15]

It is a further challenge to investigate the conditions of photodynamic equilibration of two emitting species (conformers), if their fluorescence bands are not separated but overlap strongly. Similar fluorescence energies (ν_f) of two excited state species can result either from similar absolute potential energies (E) or in case they are different from the counteracting effect of Franck−Condon ground state energies (ΔE_{FC}). Various methods, such as the maximum entropy method,[19,20] principal component analysis,[21−23] global compartmental analysis[24,25] or the concept of decay and species associated spectra[26−28] have recently been developed to analyze such phenomena.

SCHEME 1: Molecular Structures and AM1-Calculated Ground State Twist Angles φ of Donor−Acceptor Biphenyls

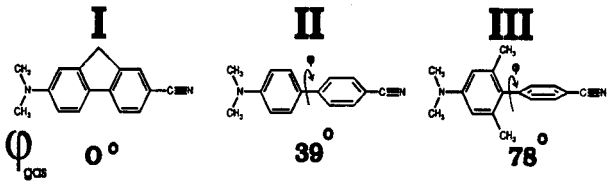

In the series of the donor−acceptor biphenyls **I**−**III** (Scheme 1), a biexponential fluorescence decay behavior on a subnanosecond time scale was found for **III** in medium polar solvents.[29−31] It has been interpreted with a dynamic excited state equilibrium between two charge-transfer species denoted as CT and the more relaxed product species CTR.[29−31] It was suggested[29] to analyze the excited state kinetics on the basis of a two-species Birks scheme where the observed two decay times τ_1 and τ_2 are described by[12,14,15,32]

$$\tau_{1,2}^{-1} = \frac{1}{2}(X + Y \pm \sqrt{(X - Y)^2 + 4k_{\mathrm{CT}\rightarrow\mathrm{CTR}}k_{\mathrm{CT}\leftarrow\mathrm{CTR}}}) \quad (1)$$

$$X = \tau_0(\mathrm{CT})^{-1} + k_{\mathrm{CT}\rightarrow\mathrm{CTR}} \qquad Y = \tau_0(\mathrm{CTR})^{-1} + k_{\mathrm{CT}\leftarrow\mathrm{CTR}} \quad (2)$$

On the other hand, time-resolved transient absorption[33] revealed that the Franck−Condon excited state (^{1}FC) should be included as a third and primary kinetic species (FC in Scheme 2) to describe the photoprocesses adequately.[5] Excitation to a ^{1}FC state that is different from the emitting state, of course, always occurs. It is just a question of how fast is the ^{1}FC relaxation in relation to the photodynamics afterward. If it is fast enough, which is, e.g., the case in the well-known dual fluorescing compound DMABN, the model of two excited species can still

† Part of the special issue "Noboru Mataga Festschrift".

10.1021/jp012432h CCC: $22.00
Published on Web 12/04/2001

SCHEME 2: Kinetic Model for I−III[a]

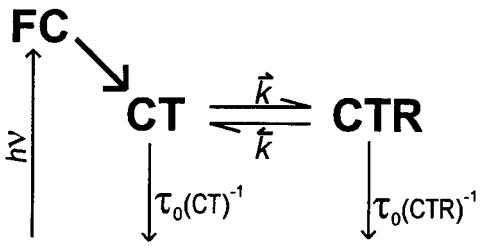

[a] The FC → CT interconversion is more than two magnitudes of order faster than the photoreaction ($k_{CT\rightarrow CTR}$, $k_{CT\leftarrow CTR}$) or ground state deactivation ($\tau_0(CT)^{-1}$, $\tau_0(CTR)^{-1}$) rate constants. The CT → CTR photoreaction occurs only for **III**.

be applied to analyze the kinetics. A further requirement to solve the Birks equations (1) and (2) for an intramolecular photoreaction by well-known methods[14,15,24−28] analyzing the amplitudes of biexponential fluorescence decays is that only the precursor species, here CT, is initially populated by FC and is emitting in the blue wing and that the product is initially absent.[34]

The time-resolved transient absorption experiments in ref 5 supported this idea for room-temperature conditions. Taking into account previous fluorescence results,[29−31] it was concluded that within a few picoseconds, a solvent-independent structural relaxation to a conformation with improved π-electron delocalization and connected with a more planar structure takes place for **I**−**III**. This process is responsible for the subsequent population of only the more emissive and more planar CT species instead of the less emissive CTR species for **II**. In the case of **III**, however, there is an excited state equilibrium between the two charge-transfer species CT and CTR, which is quantitatively analyzed (see below) by a special global analysis method adapted from Löfroth[27] to yield the separated fluorescence bands as well as the relevant kinetic and thermodynamic information.

2. Experimental Section

Materials. The synthesis of the donor−acceptor biphenyls **I**−**III** is described elsewhere.[29] Spectroscopic grade diethyl ether solvent (EOE) was purchased from MERCK (UVASOL).

Steady State Spectra. The absorption spectra presented were recorded on an ATI UNICAM UV4 UV/vis spectrophotometer. All steady state corrected spectra were obtained on an Aminco Bowman 2 fluorometer using a 150 W Xe lamp, 2 nm excitation and emission band-pass, and a photomultiplier tube in a right-angle geometry. The fluorescence spectra were corrected and converted from the recorded wavelength scale $I_f(\lambda_f)$ to a linear energy scale according to $I_f(\nu_f) = I_f(\lambda_f)\lambda^2$.

Fluorescence Quantum Yields. The quantum yields at 298 K were measured relative to quinine bisulfate in 0.1 N H_2SO_4 and calculated on the basis of[35]

$$\Phi_f = \Phi_f^{ref} \cdot \frac{n_{ref}^2}{n^2} \frac{OD^{ref}}{OD} \frac{\int I_f(\lambda_f)\, d\lambda_f}{\int I_f^{ref}(\lambda_f)\, d\lambda_f} \qquad (3)$$

where n_{ref} and n are the refractive indices of the solvents, OD^{ref} and OD (≤ 0.1) are the optical densities, Φ_f^{ref} (=52%)[36] and Φ_f are the quantum yields, and the integrals denote the (computed) area of the corrected fluorescence bands, each parameter for the standard (ref) and sample solution, respectively. The relative experimental error of the quantum yields is estimated around ±5%.

Low-Temperature Measurements. Temperature dependent fluorescence decays and spectra are measured with a homemade cooling apparatus that allows us to simultaneously freeze and control the temperature of four samples in quartz cuvettes by pumping cold nitrogen gas through the cryostat. The temperature precision and stability decreases with cooling and is estimated to be better than 2 K down to 185 K. The reproducibility of the temperature and fluorescence decays was checked in different cooling cycles. The lowest temperature achieved was about 100 K with a stability of better than 5 K. Here, diethyl ether at temperatures in the liquid phase was studied. The temperature dependent relative fluorescence intensities $I_f(T)$ are corrected for the linear increase of the refractive index $n(T)$[37] and density $\rho(T)$[37] of diethyl ether relative to room-temperature conditions by $I_f(T) = I_f(298\ K) \times \rho(298\ K) \times n(298\ K)^{-1} \times \rho(T)^{-1} \times n(T)$. The absolute error of the low-temperature fluorescence quantum yields ($\Phi_f(T)$) determined from the integrated intensity area relative to the values at room temperature is estimated to be 10%.

Fluorescence Decay Times. Synchrotron radiation from the Berlin synchrotron facility BESSY was used as light source in conjunction with an excitation monochromator (Jobin Yvon, ≈20 nm band-pass). It delivers a 4.8 MHz pulse train with characteristic pulse widths of 600 ps. Emission was detected using a time-correlated single photon counting setup.[38] It consists of a filter polarizer in the magic angle position, an emission monochromator (Jobin Yvon, ≈20 nm band-pass), and a microchannel plate photomultiplier (Hamamatsu R1564-U-01, 35 ps fwhm) cooled to −30 °C. Using standard NIM electronics from ORTEC, at most 0.1% of the excitation rate (≈5 kHz) was sampled in 1024 channels of a multichannel analyzer (ORTEC-Norland 5590) with a channel width of either 25 or 50 ps. The decays were analyzed by the "least squares" and iterative reconvolution method on the basis of the Marquardt−Levenberg algorithm, which is implemented in the commercial global analysis program.[38,39] This reconvolution technique allows an overall time resolution down to 100 ps. The quality of the exponential fits was evaluated by the reduced χ^2 value (≤ 1.2), and the autocorrelation of the residuals was quantified by the Durbin−Watson parameter ($1.9 < DW < 2.1$).[38] The minimum set of parameter to achieve a global χ^2 below 1.2 for the decays of **III** at all temperatures needs free time shifts, two linked decay times and variable amplitudes. However, to further improve the fit of those decays obtained below 180 K in the very blue wing of the spectrum, where emission intensity is low, a short time component of about 100 ps was added. This time component of weak intensity (yield less than 2%) can be due to unfavorable count statistics, stray light, or more probably solvation effects (of CT). Since it is similarly observed for all three investigated compounds, the kinetic model applied for **III** is not affected and it is therefore ignored in the analysis.

3. Results and Discussion

3.1. Global Analysis of Temperature-Dependent Emission Decays. The fluorescence of both reference compounds **I** and **II** in diethyl ether between 298 and 168 K decays monoexponentially with a lifetime of around 1.7 ns. This demonstrates that the initial relaxation FC → CT (Scheme 2) toward a more planar conformation is faster than the time resolution of 100 ps even at the lowest temperature used. The same behavior can be assumed for the more twisted biphenyl **III**, which means that within 100 ps the excited state population is described by the

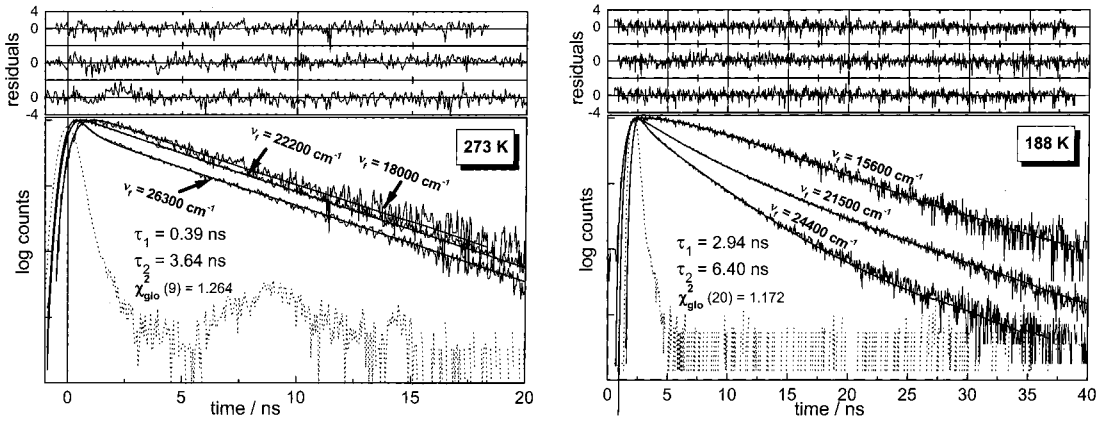

Figure 1. Emission wavenumber dependent fluorescence time traces of **III** in EOE at 273 and 188 K and their globally fitted curves. The response function is drawn in dotted lines and the residuals (fit quality parameter) are plotted in the upper boxes (at top for the smallest wavenumber ν_f).

TABLE 1: Fit Results of the Temperature Dependent Global Analysis Procedure (See Figure 2)

T (K)	decays[a]	χ^2_{glo}	τ_1 (ns)	τ_2 (ns)	α_1(blue)[b]	α_1(red)[b]	X (ns^{-1})[c]	Y (ns^{-1})[c]
273	9	1.264	0.39	3.64	0.64	−0.42	1.86	1.0
248	13	1.147	0.78	4.23	0.77	−0.35	1.06	0.45
223	7	1.094	1.33	4.97	0.87	−0.44	0.66	0.30
188	20	1.172	2.94	6.40	0.93	−0.38	0.33	0.17
168	13	1.179	3.76	7.42	0.97	−0.29	0.26	0.14

[a] Number of decay curves analyzed globally. [b] Relative amplitudes obtained in the extreme blue and red part of the emission spectrum. It is important to note that these are not extrapolated values. [c] Obtained from eq 9.

more planar CT conformer species. This is consistent with our previous results[5,29] and is further analyzed in more detail elsewhere.[40,41] On the other hand, in addition to the nanosecond single-exponential fluorescence decays, slow photodynamics, which are absent in **I** and **II**, are observed for the highly twisted biphenyl **III** by temperature and detection wavenumber dependent biexponential fluorescence decays (see below and Figure 1). This phenomenon is due to the dual emission of **III**, as described in more detail in ref 29. Emission occurs from the primarily populated more planar CT conformer species and, after a relaxation on the nanosecond time scale (adiabatic photochemical reaction) from the more twisted successor CTR species.

On the basis of the boundary condition that only the precursor species CT in the two excited species Birks Scheme 2 is populated after photoexcitation, the kinetic analysis concept of Löfroth[27] is applied to obtain the species associated fluorescence spectra, $SAS_{CT}(\nu_f)$ and $SAS_{CTR}(\nu_f)$, and the rate constants for the forward and backward reaction, $k_{CT\rightarrow CTR}(T)$ and $k_{CT\leftarrow CTR}(T)$ of the CT/CTR excited state equilibrium of **III** in EOE at different temperatures. Therefore, a set of fluorescence decays $I_f(t,\nu_f)$ for a given temperature were recorded at several wavenumbers ν_f and simultaneously fitted to a biexponential function with linked decay times τ_1 and τ_2 (eq 4) by the global analysis technique.[26,27,39]

$$I_f(t,\nu_f) = \alpha_1(\nu_f)e^{-t/\tau_1} + \alpha_2(\nu_f)e^{-t/\tau_2} \qquad (4)$$

Typical decay curves and their biexponential fits shown in Figure 1 as well as the temperature-dependent fitting results collected in Table 1 demonstrate that (i) a monoexponential model fails for **III** (but not for **II**), (ii) the biexponential model with two linked lifetimes is sufficient to achieve acceptable fit quality parameters across the entire fluorescence band, (iii) the wavenumber dependence of the decays is due to a variation of the amplitudes $\alpha_1(\nu_f)$ and $\alpha_2(\nu_f)$, (iv) the decay times, in particular the short one τ_1, become longer with cooling, and (v) τ_1 is observed as rise time in the red part of the spectra.

The temperature-dependent data sets of wavenumber dependent amplitudes and linked decay times are then analyzed by the procedure illustrated in Figure 2 for a representative temperature (T = 188 K). In Figure 2a, the relative amplitudes corresponding to the short decay time τ_1 and the longer decay time τ_2 are plotted versus the wavenumber ν_f. A large and continuous variation of the amplitudes is found, which is a signature for two excited state species emitting a smooth and structureless spectrum. The constant α values in the blue wing of the fluorescence spectrum indicate that only the precursor species is emitting there, whereas for other wavenumbers, considerable spectral overlap between CT and CTR occurs. The observation of negative amplitudes (rise times) in the low-energy region is very important, because it unambiguously proves that a photoreaction from one excited species or distribution to another one takes place. If they were not observed, the two decay times could simply be due to two nonreactive species or a single distribution of varying decay times. The consecutive reaction scheme is further supported by the fact that the observed decay times are distinctly different and show a sizable variation with temperature. Moreover, the absence of excitation wavenumber dependence for the temperature T = 183 K was checked by globally analyzing the decays obtained in the absorption range between 29 400 and 33 300 cm^{-1} at the emission wavenumbers 25 000, 21 700, and 18 000 cm^{-1}, as well as by the corresponding steady state measurements. These experiments substantiate that the two decay times are not due to more than one stable ground state species and give further support to the view that the initial Franck−Condon relaxation is sufficiently fast to populate exclusively CT instead of CTR. However, we have to note that the optimum value α_1(red) = −0.5 (or α_2/α_1(red) = −1),[34] which would evidence the complete absence of primary CTR population,[14,32] is not reached (Table 1). The fact that the

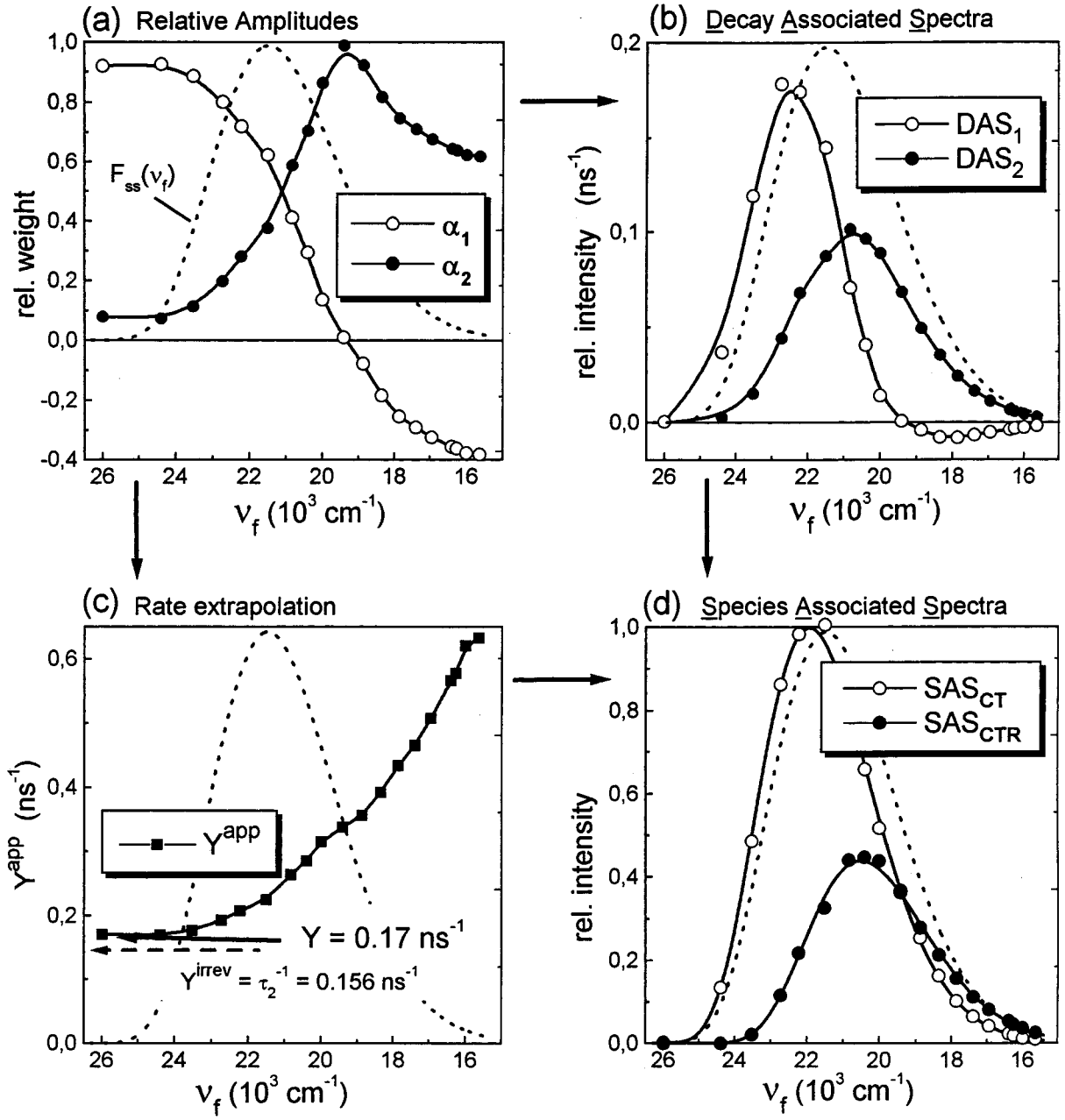

Figure 2. Diagram of the procedure to derive the photoreaction rate constants and species associated emission spectra from the global analysis results of wavenumber dependent emission decays using the results for **III** in EOE at 188 K. The broken line represents the measured steady state spectrum $F_{ss}(\nu_f)$. For more details, see text.

amplitudes or their ratios do not converge in the red edge indicates that there is still spectral overlap of the CT and CTR emission spectrum (vide infra Figure 3), which in turn can explain the values of $|\alpha_1(\text{red})|$ somewhat lower than 0.5. It may be pointed out that extrapolation of relative amplitudes $\alpha_1(\nu_f)$ toward $\nu_f = 0$ resulting in even less negative values has been reported in the literature for photoreactions where direct excitation of the product species is unlikely, too.[17,35,42] Following the convenient normalization of the amplitude spectra $\alpha_i(\nu_f)$ with the steady state spectrum $F_{ss}(\nu_f)$ suggested elsewhere,[26−28] the decay associated spectra $DAS_i(\nu_f)$ are simply obtained by[26]

$$DAS_i(\nu_f) = \frac{\alpha_i(\nu_f)}{\sum_i \alpha_i(\nu_f)\tau_i} F_{ss}(\nu_f) \quad (5)$$

So far, all interpretations are independent of the kinetic model. However, to obtain the fluorescence contributions of the species associated spectra $SAS_{CT}(\nu_f)$ and $SAS_{CTR}(\nu_f)$ at wavenumbers ν_f

$$SAS_{CT}(\nu_f) = F_{ss}(\nu_f)\frac{\int_0^\infty I_f^{CT}(\nu_f,t)\,dt}{\int_0^\infty I_f(\nu_f,t)\,dt}$$

$$SAS_{CTR}(\nu_f) = F_{ss}(\nu_f)\frac{\int_0^\infty I_f^{CTR}(\nu_f,t)\,dt}{\int_0^\infty I_f(\nu_f,t)\,dt} \quad (6)$$

the assumption of a specific kinetic scheme is necessary. Assuming ultrafast depopulation of FC, we can apply Scheme

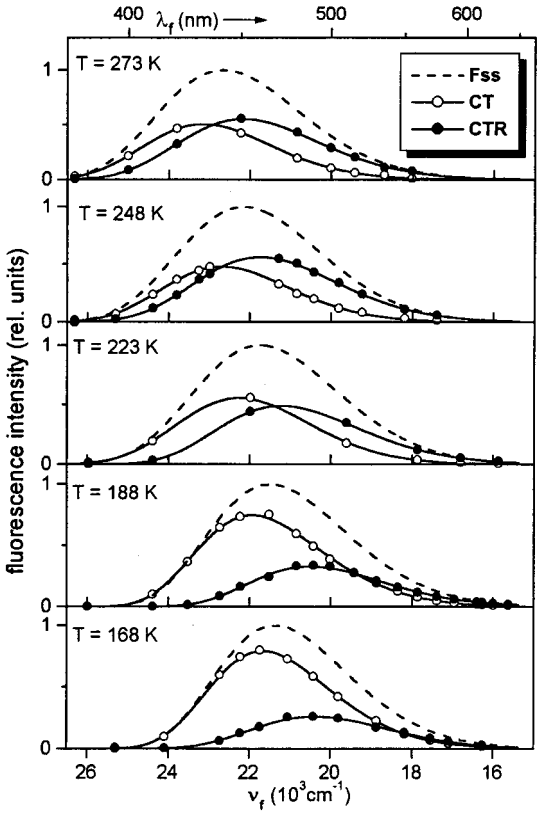

Figure 3. Species associated fluorescence spectra of CT and CTR and the corresponding steady state spectra F_{ss} (- -) for **III** in EOE.

2, leading to the following numerical expressions according to Löfroth:[27]

$$SAS_{CT}(\nu_f) = [DAS_1(\nu_f) + DAS_2(\nu_f)]\tau_1\tau_2 Y \qquad (7)$$

$$SAS_{CTR}(\nu_f) = [(\tau_1^{-1} - Y)DAS_2(\nu_f) + (\tau_2^{-1} - Y)DAS_1(\nu_f)]\tau_1\tau_2 \qquad (8)$$

where Y is defined by eq 2. In a spectral region, where only the precursor species CT emits, $SAS_{CT}(\nu_f)$ in eq 7 can be substituted by the steady state intensity $F_{ss}(\nu_f)$. Consequently, by rearranging eq 8, a plot of the apparent value $Y^{app}(\nu_f)$ across the emission spectrum

$$Y^{app}(\nu_f)^{-1} = \frac{DAS_1(\nu_f) + DAS_2(\nu_f)}{F_{ss}(\nu_f)}\tau_1\tau_2 = \frac{\alpha_1(\nu_f) + \alpha_2(\nu_f)}{\alpha_1(\nu_f)\tau_1 + \alpha_2(\nu_f)\tau_2}\tau_1\tau_2 \qquad (9)$$

can be constructed, which converges to the true value of Y at high wavenumbers, if the emission contribution of CTR approaches zero at this end of the spectrum. The plot of Y^{app} vs ν_f for **III** in EOE indeed reaches a plateau (Figure 2c) toward the blue side of the emission spectrum for all temperatures. Hence, the remaining unknown values Y and $X = \tau_1^{-1} + \tau_2^{-2} - Y$ (cf. eqs 1 and 2) for Scheme 2 are determined from $Y = Y^{app}(\nu_f \rightarrow \nu_f^{blue})$.

It may be interesting to note that this procedure to obtain Y gives the same results as a plot of the frequently used[13−15] ratio DAS_2/DAS_1 ($=\alpha_2/\alpha_1$) vs the blue emission edge (eq 10) in the case of strong reversibility or small spectral overlap of the two bands.[34]

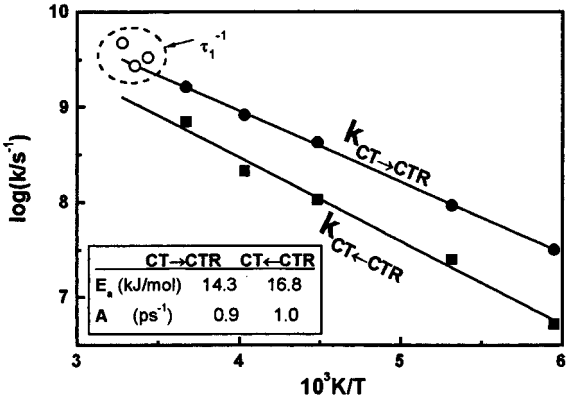

Figure 4. Arrhenius plots of forward and backward reaction rate constants. The derived activation parameters are given in the inset.

$$\frac{DAS_2}{DAS_1}(\nu_f \rightarrow \nu_f^{blue}) = \frac{\tau_2^{-1} - Y}{Y - \tau_1^{-1}} \qquad (10)$$

However, the plot of Y^{app} is superior to that of the DAS ratio in the (present) case of partial overlap and irreversibility (low DAS_2 or α_2 at ν_f^{blue}) because Y^{app} converges already at lower ν_f connected with lower derivatives $dY^{app}/d\nu_f$ than $d(DAS_2/DAS_1)/d\nu_f$.

In Figure 2c, the value of $Y^{irr} = \tau_2^{-1} = 0.156$ ns^{-1} for the model of a purely irreversible case is indicated. Its small difference from the obtained value $Y = 0.17$ ns^{-1} reveals that the photoreaction CT → CTR is in the irreversible regime. Using $Y = Y^{app}(\nu_f \rightarrow n_f^{blue})$, we can calculate the $SAS_{CT}(\nu_f)$ and $SAS_{CTR}(\nu_f)$ values (points in Figures 2d and 3). The complete SAS spectra (lines in Figure 3) are obtained by nonlinear least-squares fitting of the SAS values (points in Figure 3) to a log-normal function $I_f(\nu_f)$ of the form given in[36]

$$I_f(\nu_f) = I_f^{max}\exp\left[-\ln(2)\left\{\frac{\ln(1 + 2\gamma(\nu_f - \nu_f^{max})/\Delta)}{\gamma}\right\}^2\right] \qquad (11)$$

where I_f^{max} and ν_f^{max} are intensity and wavenumber of the emission maximum and Δ and γ are width and asymmetry parameters.

Finally, the Birks equations (1) and (2) can be completely solved, if the CT fluorescence lifetime $\tau_0(CT) = 4.3$ ns is employed, which corresponds to the decay time τ_1 at the glass transition temperature ($T_g \approx 160$ K) where the photoreaction CT to CTR and backward can be assumed to be suppressed by the high viscosity.[29] The forward and backward reaction rates can then be calculated from eqs 1 and 2 by

$$k_{CT\rightarrow CTR} = \tau_1^{-1} + \tau_2^{-1} - Y - \tau_0(CT)^{-1} \qquad (12)$$

$$k_{CT\leftarrow CTR} = (\tau_1^{-1} - Y)(\tau_2^{-1} - Y)Y^{-1} \qquad (13)$$

The temperature-dependent SAS spectra and the Arrhenius plot of the reaction rate constants are shown in Figures 3 and 4.

3.2. Quantitative Characterization of the Excited State Conformational Equilibrium between Two Charge-Transfer Species CT and CTR. *Changeover from Kinetic to Thermodynamic Control*. From integration of the SAS spectra in Figure 3, the fluorescence quantum yields of the CT and CTR species are calculated and reported in Table 2. The quantum yield Φ_f^{CTR}

TABLE 2: Ratios of CTR to CT Fluorescence Quantum Yields, Radiative Rate Constants, and Time-Integrated Excited State Concentrations for III in EOE

T (K)	$f(\epsilon_r)$[a]	η (cP)[b]	Φ_f^{CTR} (%)	Φ_f^{CT} (%)	Φ_f^{CTR}/Φ_f^{CT}	k_f^{CTR}/k_f^{CT}	[CTR]/[CT]
273	0.36	0.29	25	20	1.2	0.7	1.7
248	0.37	0.39	25	19	1.3	0.7	1.9
223	0.39	0.65	22	24	0.9	0.6	1.5
188	0.41	1.12	16	34	0.5	0.8	0.6
168	0.42	1.89	14	41	0.3	0.9	0.3

[a] Onsager polarity function $f(\epsilon_r) = (\epsilon_r - 1)/(2\epsilon_r + 1)$ using static dielectric constants ϵ_r from ref 47. [b] Viscosities from ref 46.

TABLE 3: Thermodynamic Data for the CT → CTR Photoreaction

ΔH (kJ/mol)	ΔS [(J/K)/M]	ΔG(298 K) (kJ/mol)	T_c[a] (K)	E_a (kJ/mol)	$\Delta\nu_f$[b] (cm^{-1})	$\Delta(\Delta E_{FC})$ (kJ/mol)
−2.5	−0.7	−2.3	265	14	850	7.5

[a] Changeover temperature from kinetic to thermodynamic control. [b] From solvatochromic plot in Figure 5 using ϵ_r and n at 298 K.

of the product species CTR and the ratio Φ_f^{CTR}/Φ_f^{CT} increases from 168 to 248 K, which corroborates the conclusion that the yield of the CT → CTR photoreaction is enhanced with increasing temperature. At 273 K, however, the ratio Φ_f^{CTR}/Φ_f^{CT} is lower than at 248 K. Although the observed effect is just barely outside of the experimental error, this indicates the changeover from kinetic to thermodynamic control of the excited state equilibrium above 270 K. This means that above 270 K, the backward reaction $k_{CT\leftarrow CTR}$ becomes competitive with the nonradiative deactivation of CTR, $\tau_0(CTR)^{-1}$, to the ground state (S_0).[10,11,12,14] Accordingly, the backward reaction rate constant $k_{CT\leftarrow CTR}$ (Figure 4) reaches a similar magnitude as the inverse decay time τ_2^{-1} ($10^{8.4}$ s^{-1}) at 270 K. Furthermore, a plot of the fluorescence quantum yield Φ_f as a function of the temperature T shows a minimum at ≈265 K,[40,41] which is therefore also a signature for the changeover (at T_c in Table 3) from the irreversible reaction mechanism ($T < T_c$) to the reversible reaction mechanism ($T > T_c$, equilibration reached during the excited state lifetime) where the back population of the CT species leads to an increase of Φ_f. To refine the above conclusions, the species associated fluorescence quantum yields can be expressed by[11]

$$\Phi_f^{CT} = \frac{k_f^{CT}}{X} \tag{14}$$

$$\Phi_f^{CTR} = \frac{k_{CT\rightarrow CTR} k_f^{CTR}}{XY} \tag{15}$$

in the predominantly irreversible kinetic regime, and in the reversible regime by

$$\Phi_f^{CT} = \frac{k_f^{CT} Y}{XY - k_{CT\rightarrow CTR} k_{CT\leftarrow CTR}} \tag{16}$$

$$\Phi_f^{CTR} = \frac{k_f^{CTR} k_{CT\rightarrow CTR}}{XY - k_{CT\rightarrow CTR} k_{CT\leftarrow CTR}} \tag{17}$$

if an effective two-state model with the conversion efficiencies $\eta_{FC\rightarrow CT} \cong 1$ and $\eta_{FC\rightarrow CTR} \cong 0$ is assumed (Scheme 2). Independent of which of the two kinetic regimes holds, the ratio of the CTR to CT quantum yields is given by

$$\frac{\Phi_f^{CTR}}{\Phi_f^{CT}} = \frac{k_f^{CTR}}{k_f^{CT}} \frac{k_{CT\rightarrow CTR}}{Y} = \frac{k_f^{CTR}}{k_f^{CT}} \frac{[CTR]}{[CT]} \tag{18}$$

with $k_{CT\rightarrow CTR}$ (Figure 4) and Y (Table 1) from the kinetic analysis, which consequently allows us to calculate the ratio of the CTR to CT radiative rate constants (k_f^{CTR}/k_f^{CT}) and the time-integrated concentration ratios ([CTR]/[CT] = $\int$[CTR](t) dt/$\int$[CT](t) dt).

It is found (Table 2) that the ratio of the radiative rate constants k_f^{CTR}/k_f^{CT} (0.7 ± 0.2) is smaller than unity, which characterizes the CTR species as less emissive than the CT species.[43] On the other hand, the concentration ratio [CTR]/[CT] sizably decreases with cooling after an initial increase of [CTR]/[CT] from higher temperature down to 248 K in the thermodynamically controlled temperature region ($T > T_c$). The peculiar temperature dependence of the band shape analysis parameters for **III** in EOE above 250 K as reported elsewhere is in this context also explainable with the temperature-dependent population ratio [CTR]/[CT].[40,41]

Activation Barrier of the CT → CTR Reaction. The Arrhenius plot of the reaction rate constants in Figure 4 yields activation barriers of about of E_a(CT→CTR) = 14 kJ/mol for the forward and E_a(CTR→CT) = 17 kJ/mol for the backward reaction. They are significantly larger than the activation energy for the solvent mobility of EOE (E_η = 7 kJ/mol) and the measured Arrhenius barrier of DMABN (E_a(LE→CT) = 4 kJ/mol),[13] demonstrating the existence of a high intrinsic reaction barrier ($E_i^{\#}$) beside a possible "viscosity barrier" induced by solvent drag.[44] The latter conclusion is supported by a comparison of temperature and pressure dependent experiments.[40,45] The slightly different Arrhenius barrier derived previously (E_a = 15 kJ/mol)[29] assuming purely irreversible kinetics is close to the present value of the detailed analysis, because the reaction mechanism is in fact predominantly irreversible.

Thermodynamics of the Excited State Reaction. The CT → CTR reaction enthalpy, ΔH, and entropy, ΔS, the free reaction enthalpy, ΔG, at 298 K, and the difference between the CTR and CT Franck−Condon ground state energy $\Delta(\Delta E_{FC})$ are calculated by eqs 19−22 (see Table 3 and Scheme 3).

$$\Delta H = E_a^{CT\leftarrow CTR} - E_a^{CT\rightarrow CTR} \tag{19}$$

$$\Delta S = R(\ln k_{CT\rightarrow CTR}^{T\rightarrow\infty} - \ln k_{CT\rightarrow CTR}^{T\rightarrow\infty}) \tag{20}$$

$$\Delta G(T) = -RT \ln \frac{k_{CT\rightarrow CTR}(T)}{k_{CT\leftarrow CTR}(T)} \tag{21}$$

$$\Delta(\Delta E_{FC}) = \Delta H - hc\Delta\nu_f \tag{22}$$

It is noteworthy that ΔG(298 K) is small and close to RT (2.5 kJ/mol at 298 K), which agrees well with the estimation derived previously.[29] Moreover, the change of the enthalpy ΔH (or the change of the potential energy by the reaction CT → CTR) is also small and much less than that reported for DMABN in

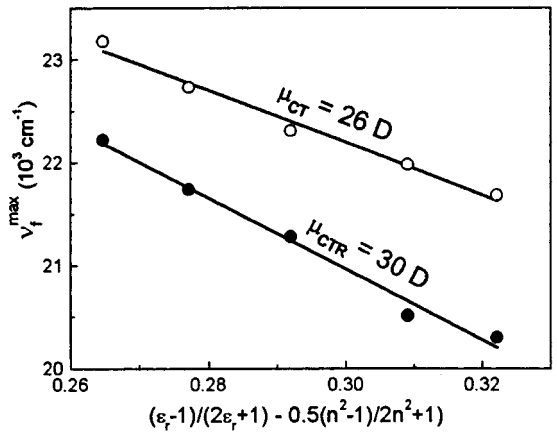

Figure 5. Lippert−Mataga plot to obtain species associated dipole moments of CT and CTR.

SCHEME 3: Potential Energy Diagram of S_0 and S_1 for the Photoreaction of III in EOE from CT to CTR in the Solvent Relaxed $^1CT(S_1)$ State

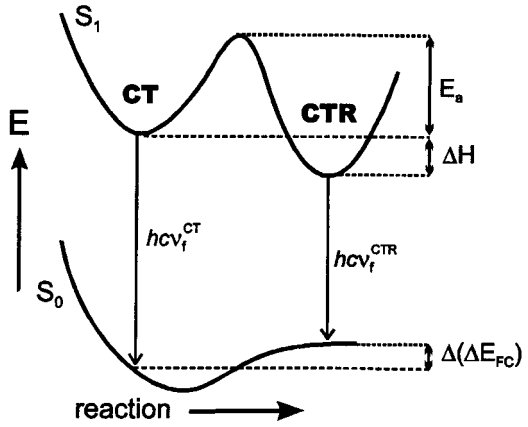

toluene (−10 kJ/mol)[14] or in EOE (−17 kJ/mol).[13] The reason for this large difference in the reaction enthalpy ΔH between **III** and DMABN is due to the fact that for DMABN, a transformation occurs from a locally excited state ^{1}LE (μ_e < 9.9 D)[15] to a ^{1}CT state (μ_e = 17 D),[15] which is strongly stabilized by the solvent, whereas the photoreaction of **III** takes place on a ^{1}CT potential surface where the electron-transfer character along the reaction path increases only slightly (see further discussion below).

Dipole Moments of CT and CTR. The excited state dipole moments μ_e of the CT and CTR species are quantified in Figure 5 by a solvatochromic plot according to Mataga (eq 23)[46] of the emission maxima $\nu_f(T)$ obtained from the log-normal fits (eq 11) of the SAS_{CT} and SAS_{CTR} values in Figure 3.

$$\nu_f(T) = \nu_f^{gas}(T) - \frac{2\mu_e(\mu_e - \mu_g)}{hca^3}\left(\frac{\epsilon_r(T)-1}{2\epsilon_r(T)+1} - 0.5\frac{n^2(T)-1}{2n^2(T)+1}\right) \quad (23)$$

In eq 23 $\epsilon_r(T)$ and $n^2(T)$ denote the temperature-dependent static dielectric constants and the squared refractive index of EOE, respectively.[37,47]

The increase of the dipole moment from CT (μ_{CT} = 26 D) to CTR (μ_{CTR} = 30 D) amounts to 4 D only, revealing the slight increase of ^{1}ET character accompanied by the photoreaction. Further, these values are consistent with the average dipole moment ($\langle m_e \rangle$ = 27.6 D) obtained previously by steady state emission in different solvents.[29] This finding together with the larger radiative rate k_f of CT is in agreement with the previous assignment of CT to a more planar and CTR to a more twisted rotamer, as compared to the average conformation in S_0.

Influence of Solvent Polarity, Viscosity, and Temperature. One might ask about the influence of the solvent properties such as solvent polarity (see $f(\epsilon_r)$ in Table 2) and viscosity (see η in Table 2), which both increase with decreasing temperature. The increase of the polarity preferably stabilizes the more polar CTR species and thus could be expected to lead to an acceleration of the CT → CTR reaction connected with decreasing emission yield. But the opposite behavior is observed, since the change of polarity for the chosen conditions is only small as compared to the strong increase of viscosity for a decrease of temperature (Table 2). Due to the increase of the excited state dipole moment along the CT → CTR path the polarity effect alone reduces the observed barrier, which supports the existence of a high intrinsic barrier. On the other hand, with regard to the interpretation that an intramolecular twisting motion is involved in the photoreaction, a slowing down of the rates by the solvent viscosity is very probable and would therefore lead to an apparently higher thermal barrier. As shown elsewhere by high-pressure measurements, the viscosity is indeed able to slow this photoreaction.[40,45]

Even though the viscosity effect is not negligible, the temperature is the dominating factor for the photoreaction rates, as evidenced by the comparison of temperature with pressure dependent fluorescence experiments.[40,45] Consequently, the observed energy barrier and the separated properties of the photoreactive species are in agreement with previous calculation results, where a barrier crossing process has been postulated only for **III** in medium polar solvents, leading from a more planar to a more twisted structure as compared to the ground state situation.[29]

4. Conclusions

The thermodynamics and the kinetics of the adiabatic photoreaction occurring between two CT species in the strongly twisted donor−acceptor biphenyl **III**, but not in the planar and slightly twisted compounds **I** and **II**, are quantitatively determined by a global fluorescence decay analysis method. Since the photoreaction is associated with (i) an increase of the dipole moment from 26 to 30 D and (ii) a decrease of the fluorescence rate constants (factor ca. 0.7), which are both intramolecular properties, the reaction coordinate can mainly be attributed to an intramolecular twisting from a more planar precursor rotamer denoted by CT to a more twisted rotamer denoted by CTR. The "R" of CTR stands for "*more relaxed*" to identify it as a photoproduct species in the ^{1}CT state that is associated with stronger ^{1}ET character than the precursor CT species.

In contrast to DMABN in EOE, separated steady state fluorescence bands are not observed for **III** in EOE, because the difference of the potential energies ΔH (**III**, −2.5 kJ/mol; DMABN, −17kJ/mol)[13] and that of the ground state reorganization energies $\Delta(\Delta E_{FC})$ (**III**, 7.5 kJ/mol; DMABN, 40 kJ/mol)[48] are similar for the charge-transfer species CT and CTR. Therefore, both emission bands occur approximately at the same wavelength. Further, a larger energy barrier E_a (**III**, 14.3 kJ/mol; DMABN,[13] 4 kJ/mol) connected with a relatively small change of free energy ΔG (at 293 K: **III**, −2.3 kJ/mol; DMABN, −6.1 kJ/mol) of **III**, is responsible for the slower (by 2 orders of magnitude!) reaction rate constants (at 293 K: **III**, $k_{CT\rightarrow CTR} = 10^{9.4}$ s^{-1}; DMABN, $k^1_{LE\rightarrow}{}^1_{CT} = 10^{10.9}$ s^{-1}) as compared to DMABN. This difference is enhanced at low temperatures.[13] The reason for these differences between the photoreaction in **III** and DMABN are due to the fact that only

the precursor species in DMABN has strongly locally excited character (significantly reduced dipole moment), such that a "steep downhill reaction" connected with a strong change of the electronic character to the more or less pure ^{1}CT state is observed in EOE. For **III**, however, the comparable "steep downhill reaction" ^{1}FC → ^{1}CT investigated in ref 5 occurs prior to the photoreaction CT → CTR, such that small energy changes and a high intrinsic barrier are found, which are characteristic of an equilibrium between two conformer species of similar electronic character.

References and Notes

(1) Aloisi, G. G.; Elisei, F.; Latterini, L.; Marconi, G.; Mazzucato, U. *J. Photochem. Photobiol. A: Chem.* **1997**, *105*, 289.

(2) Szymanski, M.; Maciejewski, A.; Kozlowski, J.; Koput, J. *J. Phys. Chem. A* **1998**, *102*, 676.

(3) Muralidharan, S.; Yates, K. *Chem. Phys. Lett.* **1992**, *192*, 571.

(4) Kovalenko, S. A.; Ernsting, N. P.; Ruthmann, J. *Chem. Phys. Lett.* **1996**, *258*, 445.

(5) Maus, M.; Rettig, W.; Jonusauskas, G.; Lapouyade, R.; Rullière, C. *J. Phys. Chem. A* **1998**, *102*, 7393.

(6) Grabowski, Z. R.; Rotkiewicz, K.; Siemiarczuk, A.; Cowley, D. J.; Baumann, W. *Nouv. J. Chim.* **1979**, *3*, 443.

(7) Rettig, W. *Angew. Chem., Int. Ed. Engl.* **1986**, *25*, 971.

(8) Dey, J.; Warner, I. M. *J. Phys. Chem. A* **1997**, *101*, 4872

(9) Rotkiewicz, K.; Rechthaler, K.; Puchala, A.; Rasala, D.; Styrcz, S.; Köhler, G. *Chem. Phys. Lett.* **1996**, *98*, 15.

(10) Rettig, W.; Chandross, E. A. *J. Am. Chem. Soc.* **1985**, *107*, 5617.

(11) Rettig, W. *J. Luminescence* **1981**, *26*, 21.

(12) Rettig, W. *J. Phys. Chem.* **1982**, *86*, 1970.

(13) Zachariasse, K.; Grobys, M.; von der Haar, T.; Hebecker, A.; Il'ichev, Yu. V.; Jiang, Y.-B.; Morawski, O.; Kühnle, W. *J. Photochem. Photobiol. A: Chem.* **1996**, *102*, 59.

(14) Leinhos, U.; Kühnle, W.; Zachariasse, K. A. *J. Phys. Chem.* **1991**, *95*, 2013.

(15) Schuddeboom, W.; Jonker, S. A.; Warman, J. M.; Leinhos, U.; Kühnle, W.; Zachariasse, K. A. *J. Phys. Chem.* **1992**, *96*, 10809.

(16) von der Haar, T.; Hebecker, A.; Il'ichev, Yu. V.; Jiang, Y.-B.; Kühnle, W.; Zachariasse, K. A. *Recl. Trav. Chim. Pays-Bas Photochem.* **1995**, *114*, 430.

(17) Albinsson, B. *J. Am. Chem. Soc.* **1997**, *119*, 6369.

(18) Kasha, M. *Discuss. Faraday Soc.* **1950**, *6*, 14.

(19) Livesey, A. K.; Licinio, P.; Delaye, M. *J. Chem. Phys.* **1986**, *84*, 5102.

(20) Livesey, A. K.; Brochon, J. C. *Biophys. J.* **1987**, *52*, 693.

(21) Lawton, W. H.; Sylvestre, E. A. *Technometrics* **1971**, *13*, 617.

(22) Saltiel, J.; Sears, D. F.; Choi, J.-O.; Sun, Y.-P.; Eaker, D. W. *J. Phys. Chem.* **1994**, *98*, 35.

(23) Spalletti, A.; Bartocci, G.; Masetti, F.; Mazzucato, U.; Cruciani, G. *Chem. Phys.* **1992**, *160*, 131.

(24) Ameloot, M.; Boens, N.; Andriessen, R.; Van den Bergh, V.; DeSchryver, F. C. *J. Phys. Chem.* **1991**, *95*, 2047.

(25) Hermans, E.; DeSchryver, F. C.; Dutt, G. B.; van Stam, J.; de Feyter, S.; Boens, N.; Miller, R. D. *New. J. Chem.* **1996**, *20*, 829.

(26) Knutson, J. R.; Walbridge, D. G.; Brand, L. *Biochemistry* **1982**, *21*, 4671.

(27) Löfroth, J.-E. *J. Phys. Chem.* **1986**, *90*, 1160.

(28) Strehmel, B.; Seifert, H.; Rettig, W. *J. Phys. Chem. B* **1997**, *101*, 2232.

(29) Maus, M.; Rettig, W.; Bonafoux, D.; Lapouyade, R. *J. Phys. Chem. A* **1999**, *103*, 3388.

(30) Maus, M.; Rettig, W.; Lapouyade, R. *J. Inf. Rec.* **1996**, *22*, 451.

(31) Rettig, W.; Maus, M. *Ber. Bunsen-Ges. Phys. Chem.* **1996**, *100*, 2091.

(32) Birks, J. B. *Photophysics of Aromatic Molecules*; Wiley-Interscience: New York, 1970.

(33) Maus, M.; Rettig, W.; Jonusauskas, G.; Lapouyade, R.; Rulliere, C. *J. Phys. Chem. A* **1998**, *102*, 7393.

(34) The ratio of the preexponential factors (or the DAS values, see eq 5) derived from ref 32 for the biexponential time dependence of the precursor emission is given by

$$\frac{\alpha_2}{\alpha_1}(\mathrm{CT}) = \frac{[\mathrm{CT}]_{t=0}(\tau_2^{-1} - Y) - [\mathrm{CTR}]_{t=0}k_{\mathrm{CT}\leftarrow\mathrm{CTR}}}{[\mathrm{CT}]_{t=0}(Y - \tau_1^{-1}) + [\mathrm{CTR}]_{t=0}k_{\mathrm{CT}\leftarrow\mathrm{CTR}}}$$

and that for the product emission by

$$\frac{\alpha_2}{\alpha_1}(\mathrm{CTR}) = \frac{[\mathrm{CTR}]_{t=0}(Y - \tau_1^{-1}) - [\mathrm{CT}]_{t=0}k_{\mathrm{CT}\rightarrow\mathrm{CTR}}}{[\mathrm{CTR}]_{t=0}(\tau_2^{-1} - Y) + [\mathrm{CT}]_{t=0}k_{\mathrm{CT}\rightarrow\mathrm{CTR}}}$$

where α_1 and α_2 are the preexponenential factors for the short and long decay time τ_1 and τ_2 (cf. eq 4) and $[\mathrm{CT}]_{t=0}$ and $[\mathrm{CTR}]_{t=0}$ are the initial relative concentrations of the CT and CTR species populated by the FC relaxation. Both equations show that the desired value of Y can only be obtained from the amplitude ratios, if $[\mathrm{CTR}]_{t=0}$ equals to zero. Otherwise, experiments with different concentrations of added quenchers that act differently on CT and CTR are necessary (refs 24 and 25). Note also that α_2/α_1(CTR) for pure CTR emission equals to -1, if $[\mathrm{CTR}]_{t=0} = 0$.

(35) Heisel, F.; Miehé, J. A. *Chem. Phys.* **1985**, *98*, 233.

(36) Fraser, R. D. B.; Suzuki, E. In *Spectral Analysis*; Blackburn, J. A., Ed.; Marcel Dekker: New York. 1970; p 171.

(37) Riddick, J. A.; Bunger, W. B.; Sakano, T. K. *Organic Solvents*; John Wiley & Sons: 1986.

(38) Connor, D. V.; Phillips, D. *Time correlated single photon counting*; Academic Press: London, 1984.

(39) Globals Unlimited, Laboratory of Fluorescence Dynamics at the University of Illinois, 1992.

(40) Maus, M. *Photoinduced Intramolecular Charge Transfer in Donor−Acceptor Biaryls and Resulting Applicational Aspects*; Dissertation.com: Parkland, 1998; ISBN 1-58112-030-3.

(41) Maus, M.; Rettig, W. *manuscript in preparation*.

(42) Yip, R. W.; Wen, Y.-W.; Szabo, A. G. *J. Phys. Chem.* **1993**, *97*, 10458.

(43) The reliability of $k_f^{\mathrm{CTR}}/k_f^{\mathrm{CT}}$ suffers mainly from a possible inaccuracy of the relative amplitudes in the spectral area of high relative fluorescence intensity. In particular, the difficulty to determine the k_f ratio of a system with a relatively small extent of the photoreaction, here at the lowest temperatures, has been stressed and discussed in detail in ref 15.

(44) Rettig, W.; Fritz, R.; Braun, D. *J. Phys. Chem. A* **1997**, *101*, 683.

(45) Maus, M.; Rettig, W. *J. Inf. Rec.* **1998**, *24* (5/6), 461.

(46) Mataga, N.; Kaifu, Y.; Koizumi, M. *Bull. Chem. Soc. Jpn.* **1956**, *29*, 465.

(47) Landolt-Börnstein. *Zahlenwerte und Funktionen aus Physik, Chemie, Astronomie, Geophysik und Technik*; Schäfer, K. H., Ed.; Springer-Verlag: Berlin, 1969; Vol. 2(5), Landolt-Börnstein, New series IV/6.

(48) For DMABN, $\Delta(\Delta E_{\mathrm{FC}}) = 73$ kJ/mol was estimated in ref 13 from $\Delta(\Delta E_{\mathrm{FC}}) = hc\nu_a(^1\mathrm{LE}) + \Delta H - hc\nu_f(^1\mathrm{CT})$ with the absorption energy $hc\nu_a$ of the ^{1}LE state. This neglects ΔE_{FC} and the stabilization energy of the ^{1}LE state. $\Delta(\Delta E_{\mathrm{FC}})$ for DMABN is therefore recalculated here by eq 22 using the experimental values in EOE[13,16] $\Delta H = -17$ kJ/mol, $\nu_f(^1\mathrm{LE}) = 28\,600$ cm^{-1} and $\nu_f(^1\mathrm{CT}) = 23\,850$ cm^{-1}. Note, that the derived value of $\Delta(\Delta E_{\mathrm{FC}})$ for **III** agrees well with the result from the band-shape analysis[40,41] using $\Delta(\Delta E_{\mathrm{FC}})/hc = [\lambda_i(\mathbf{III}\text{ in EOE}) - \lambda_i(\mathbf{III}\text{ in HEX}) + (\lambda_s + \lambda_i')(\mathbf{III}\text{ in EOE}) - (\lambda_s + \lambda_i')(\mathbf{II}\text{ in EOE})$.